Impact of cell size on morphogen gradient precision

Jan A. Adelmann[1], Roman Vetter[1, 2], and Dagmar Iber[1, 2, *]

[1] *Department of Biosystems Science and Engineering, ETH Zürich, Mattenstrasse 26, 4058 Basel, Switzerland*
[2] *Swiss Institute of Bioinformatics, Mattenstrasse 26, 4058 Basel, Switzerland*

February 2, 2022

Patterning during embryonic development is remarkably precise and reproducible. How high patterning precision is achieved is still largely elusive. Here, we use a novel simulation framework to determine the impact of cell size on the variability of morphogen gradients and the positional information they convey. We find that both variability in the cell diameter and spatial averaging of the local concentration affect the sensed gradient variability only little. In contrast, the mean cell diameter has a profound impact on gradient variability and on the resulting positional accuracy. We reveal the corresponding scaling relationships between positional error, cell diameter and gradient length. Consistent with this observation, apical cell areas are small in tissues that are patterned by morphogen gradients. We conclude that tissues achieve higher patterning precision with small cross-sectional cell areas.

1 Introduction

During embryogenesis, cells must coordinate complex differentiation programs within expanding tissues. According to the French flag model, morphogen gradients define pattern boundaries in the developing tissue based on concentration thresholds (Wolpert; 1969). Exponential functions of the form

$$C(x) = C_0 e^{-x/\lambda} \tag{1}$$

approximate the shape of measured morphogen gradients very well (Kicheva et al.; 2007; Gregor et al.; 2007, 2008; Yu et al.; 2009; Wartlick et al.; 2011, 2014; Cohen et al.; 2015; Mateus et al.; 2020). For such gradients, the positional error

$$\sigma_x = \text{stddev}\,[x_\theta]$$

of the readout positions

$$x_\theta = \lambda \ln \frac{C_0}{C_\theta}$$

in different embryos depends on the variation in the decay length λ and in the amplitude C_0 relative to the readout threshold C_θ. Strikingly, the positional error of measured morphogen gradients has been reported to exceed that of their readouts (Houchmandzadeh et al.; 2002; Gregor et al.; 2007; Zagorski et al.; 2017).

Several theories have been proposed to explain the high readout precision despite inevitable noise and variation in morphogen gradients and their readout processes. They include temporal and spatial averaging, self-enhanced morphogen turnover, and the use of opposing gradients (Houchmandzadeh et al.; 2002; Gregor et al.; 2007; Lander et al.; 2009; Morishita and Iwasa; 2009, 2011; Tkačik et al.; 2015; Zagorski et al.; 2017). In zebrafish, where cells are rather motile, cell sorting and competition can further enhance boundary precision (Xiong et al.; 2013; Akieda et al.; 2019; Tsai et al.; 2020).

A recently developed numerical framework estimates how much variability in and between morphogen gradients can be accounted for by the molecular noise reported for morphogen production, decay, and diffusion (Vetter and Iber; 2021). The predicted gradient variability is considerably lower than what has been reported. Single gradients are sufficiently precise to achieve the observed developmental patterning precision. The discrepancy between predicted and observed gradient variability could point to biological noise unaccounted for by the simple model, or to technical limitations in those very challenging experiments. We have now extended the framework to analyse the impact of cell size and spatial averaging on morphogen gradient variability, and find that positional accuracy is higher, the narrower the cells.

*Corresponding author: dagmar.iber@bsse.ethz.ch

2 Results

We approximate the patterning domain by a line, such that the cell size in our simulations corresponds to the cell diameter δ in 1D, or the cross-sectional area A in 2D in the epithelium (Fig. 1A). This allows us to evaluate the impact of cell-to-cell variability in the production, degradation and diffusion rates p, d, D, as well as in the cell cross-sectional areas A, on gradient variability (Fig. 1B, Methods). Relative variability or uncertainty of a positive quantity X is quantified by its coefficient of variation $\text{CV}_X = \sigma_X/\mu_X$, where μ_X and σ_X denote the mean and standard deviation of X, respectively. For the local concentration, this is CV_C. Alternatively, one can fit Eq. 1 to each gradient and quantify CV_λ and CV_0 of the two fit parameters λ and C_0 individually.

Cell size, but not its variability, affects gradient variability

Our simulations reveal that an increase in the average cell diameter μ_δ leads to greater variability in λ and C_0 (Fig. 1C,D), according to power laws

$$\text{CV}_\lambda \sim \left(\frac{\mu_\delta}{\mu_\lambda}\right)^\alpha \quad \text{and} \quad \text{CV}_0 \sim \left(\frac{\mu_\delta}{\mu_\lambda}\right)^\beta$$

with exponents $\alpha = 0.512 \pm 0.004$ (mean ± SEM, Fig. 1C, blue curve) and $\beta = 0.473 \pm 0.005$ (Fig. 1D, blue curve). Square-root scaling for the decay length variability ($\alpha = 0.5$) follows from the law of large numbers and is consistent with the inverse-square-root scaling reported for the dependency of CV_λ on the

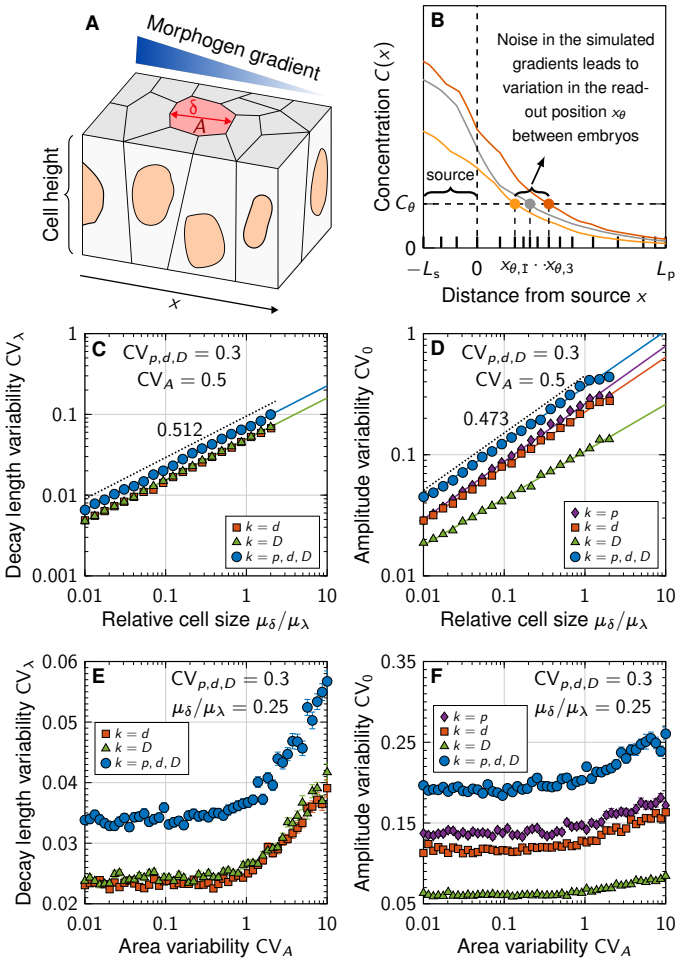

Figure 1: Cell size, but not its variability, affects gradient variability. A In our simulations, three-dimensional cells are approximated by one-dimensional intervals with lengths δ. In a tissue cross section perpendicular to cell height, δ represents the effective diameter (red double arrow) of the cell's area A (red) along the patterning axis x. **B** The domain is split into a morphogen-secreting source of length L_s and a patterning domain of length L_p. Cell boundaries are denoted by black ticks. Variability in the simulated gradients (colours) arises from differences in cell diameters (δ), morphogen production (p), degradation (d), and diffusion (D) rates in each cell and can lead to shifted readout positions $x_{\theta,i}$ for a fixed threshold concentration C_θ. **C,D** Scaling of gradient variability with the cell diameter relative to the mean decay length at fixed kinetic variability $CV_{p,d,D}$ and fixed cell area variability CV_A. Fitted power-law exponents are indicated. Mean cell diameters μ_δ were varied, mean gradient decay lengths μ_λ resulted from fitting. **E,F** Gradient variability as a function of cell area variability at fixed kinetic variability. Decay length variability (**E**) is largely unaffected by area variability as long as $CV_A < 1$ and increases only for greater values. Amplitude variability (**F**) is nearly constant over the cell area variability range considered and only increases moderately for $CV_A > 1$. Error bars are SEM.

patterning domain length L_p at fixed cell size (Vetter and Iber; 2021). Together, this suggests that

$$CV_\lambda \sim \sqrt{\frac{\mu_\delta}{L_p}} \sim \sqrt{\frac{1}{N_{cells}}}, \qquad (2)$$

where N_{cells} is the (mean) number of cells along the patterning axis. Smaller cell diameters thus lead to smaller effective morphogen gradient variability.

Cell-to-cell variability in the cross-sectional cell area A does not affect the gradient variability as long as $CV_A < 1$ (Fig. 1E,F). Only for extreme cell area variability exceeding 1, the variability in λ grows (Fig. 1E). However, we are not aware of any reported $CV_A > 1$ (Guerrero et al.; 2019; Kokic et al.; 2019; Gómez et al.; 2021; Bocanegra-Moreno et al.; 2022). Consequently, cell size has a considerable impact on gradient variability, while physiological levels of variability in the cell diameter do not contribute to gradient imprecision.

Spatial averaging results in a small shift in the readout position

Since cells can assume only a single fate, domain boundaries must follow cell boundaries (Fig. 2A). Cells may average the morphogen signal over their surface. What is then the readout position of the gradient? Assuming that cells have no orientational bias, we can approximate cell surfaces as disks with radius $r = \mu_\delta/2$ about a centre point x_0. If threshold-based readout operates on the averaged concentration, the effective readout domain boundary is shifted along the concentration gradient to $x_0 = x_\theta + \Delta x$ by the distance

$$\Delta x = \lambda \left[\frac{1}{8} \left(\frac{r}{\lambda}\right)^2 - \frac{1}{384} \left(\frac{r}{\lambda}\right)^4 + \mathcal{O}\left(\left(\frac{r}{\lambda}\right)^6 \right) \right]$$

in absence of morphogen gradient variability and cell size variability (see Supplemental Information). For $r = 2.45$ µm and $\lambda = 19.3$ µm as found for Sonic hedgehog (SHH) in the mouse neural tube (NT) (Cohen et al.; 2015), the shift is $\Delta x = 0.039$ µm, or 0.8% of the cell diameter.

In the case of rectangular rather than circular cell areas, cells are confined to the interval $[x_0 - r, x_0 + r]$. The theoretically predicted shift is then approximately 0.052 µm in the mouse NT (see Supplemental Information) or 1% of the cell diameter. This agrees with the shift we measured in our simulations, $\Delta x = 0.0523 \pm 0.0001$ µm (mean ± SEM, Fig. 2B), confirming that spatial averaging of an exponential gradient results in a higher average concentration than centroid readout. The shift is, however, small and can be neglected in the analysis of tissue patterning if $r \ll \lambda$.

Spatial averaging has little impact on the gradient variability that cells sense

Spatial and temporal averaging can reduce the overall gradient noise (Gregor et al.; 2007; Berg and Purcell; 1977; Bialek and Setayeshgar; 2005). In epithelia, receptors may either be dispersed on the apical surface, or along the baso-lateral cell surface, or, in case of hormones, be limited to nuclei (Saitoh et al.; 2013; Zhang et al.; 2019). In the mouse NT, the SHH receptor PTCH1 is restricted to a cilium located on the apical surface (Saade et al.; 2013). The range of spatial averaging then depends on the cilium length and flexibility rather than the cross-sectional cell area. We therefore tested the alternative possibilities that morphogens are sensed only at a single point per cell, that this point is either randomly located or situated at the centroid, and that the radius of sensing ranges from zero to the maximal cilium length (Fig. 2C).

While the mean cell diameter μ_δ greatly affects the gradient variability CV_C, the readout strategy has only a moderate impact (Fig. 2D). The difference is most pronounced for large cells, where the sensed morphogen variability is largest if the cellular readout point is randomly placed (Fig. 2D, blue). Readout at the centroid or averaged over the entire cell yield similar gradient variabilities, and thus readout precision. This can be understood since the theoretical considerations above predict only a small shift. Also, a cilium that averages the gradient

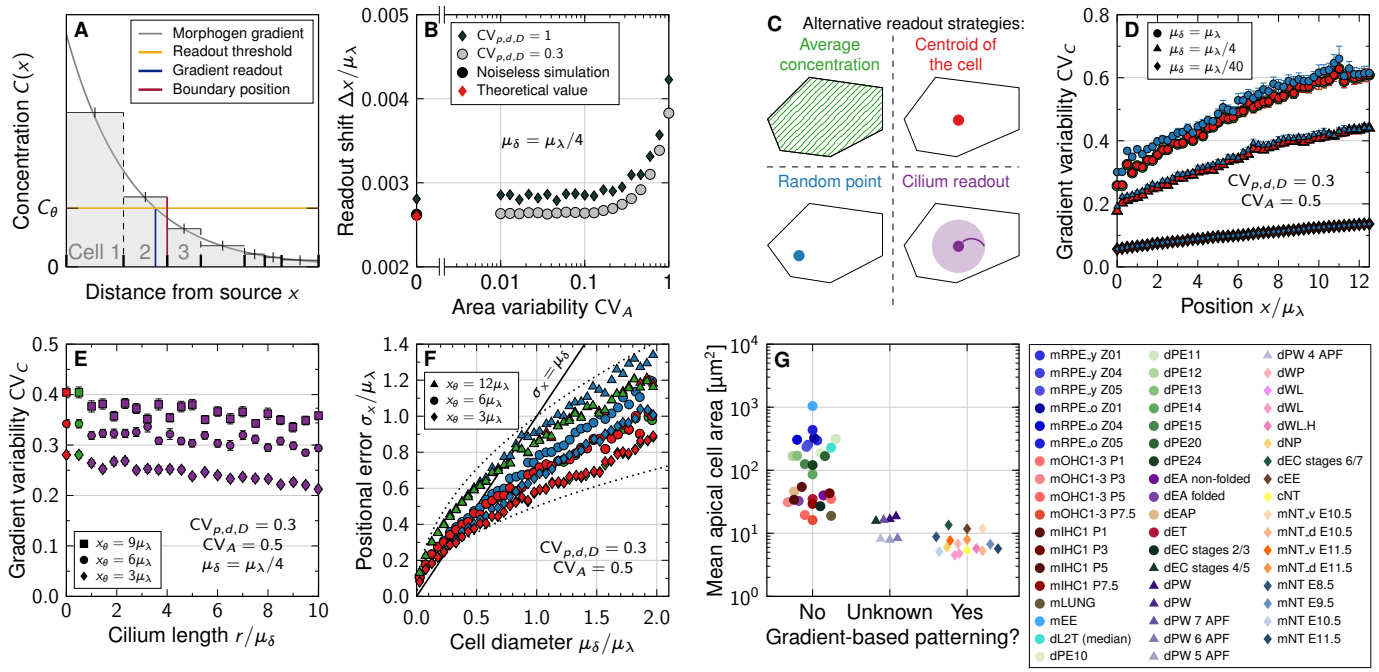

Figure 2: Impact of cell size and readout method on gradient readout precision. A Cell-based readout of a morphogen gradient (grey). A concentration threshold C_θ (yellow) defines a readout position x_θ (blue). If cells read out cell-area-averaged concentrations, the effectively sensed concentration profile is a step function. Pattern boundaries form at cell edges (red). **B** Cell-area-averaged readout results in a small shift Δx compared to readout localised to the cell centroid. Larger kinetic or area variability increases Δx. **C** Four different methods how cells may read out morphogens. Colours in panels D-F correspond to these readout mechanisms. **D** The readout methods yield almost identical relative variability in the concentration over the patterning domain for small and medium sized cells. A difference emerges only for larger cell diameters ($\mu_\delta = \mu_\lambda$). **E** Spatial averaging over a larger readout region (radius r) does not substantially decrease relative morphogen concentration variability. **F** The positional error σ_x increases with the square root of the mean cell diameter μ_δ. Dotted lines show the relationship $\sigma_x/\mu_\lambda = \gamma\sqrt{\mu_\delta/\mu_\lambda}$ for $\gamma = 1/2, 1$. **G** Tissues that use gradient-based patterning (GBP) have small mean apical cell areas (MACA). In the chick (cNT) and mouse NT (mNT) where SHH, Bone Morphogenetic Protein (BMP), and WNT gradients define the progenitor domain boundaries (Briscoe and Small; 2015), the MACAs are largely around 7 µm^2 and remain below 12 µm^2 (Guerrero et al.; 2019; Escudero et al.; 2011; Bocanegra-Moreno et al.; 2022). The chick embryonic ectoderm (cEE) appears to be patterned by BMP gradients (Pera et al.; 1999), with MACA just below 12 µm^2 (Escudero et al.; 2011). In the *Drosophila* larval notum (dNP) and wing disc (dWL), Hh, Decapentaplegic (Dpp), and Wnt gradients pattern the epithelium (Briscoe and Small; 2015; Tomoyasu et al.; 2000; Cavodeassi et al.; 2002), with MACAs < 7 µm^2 (Kokic et al.; 2019; Escudero et al.; 2011). The MACAs of the wing disc (WD) increase through the pre-pupal stages (dWP, dPW), to ≈ 18 µm^2 in the pupal stages (Kokic et al.; 2019; Escudero et al.; 2011). The Dpp gradient length increases over time (Wartlick et al.; 2011), possibly allowing ACAs to become larger at later stages, but morphogen gradients may also play less of a role in the pupal stages. In the *Drosophila* egg chamber (dEC), the MACAs decline from ≈ 30 µm^2 at stage 2/3 to ≈ 10 µm^2 by stage 6/7 (Finegan et al.; 2019), consistent with reported GBP at stage 6 (Osterfield et al.; 2017), We did not find reports of earlier GBP. While gradients pattern the *Drosophila* blastoderm syncytium (Briscoe and Small; 2015), no morphogen gradients are known during cellularisation. MACAs are reportedly in the range 35–45 µm^2 (Rupprecht et al.; 2017), much larger than in the NT or WD. For the peripodal membrane (dPE10–24) of the *Drosophila* eye disc, no GBP has been described and MACAs range from 85 µm^2 to more than 300 µm^2 (Kokic et al.; 2019). In the *Drosophila* L2 trachea (dL2T), no gradients have been reported and the MACAs are > 200 µm^2 (Skouloudaki et al.; 2019). In the mouse embryonic lung (mLUNG), no morphogen gradients have been reported, despite chemical patterning (Iber; 2021). The MACA is ≈ 19 µm^2 (Kadzik et al.; 2014). MACAs in the postnatal (P1–P21) cochlea are 15–55 µm^2 (Etournay et al.; 2010). In adult mouse retinal pigment epithelial (mRPE) cells, the MACAs exceed 200 µm^2 in young mice (P30) and increase to > 400 µm^2 in old mice (P720) (Kim et al.; 2021). In the *Drosophila* embryo AP (dEAP), the MACA is ≈ 46 µm^2 and in the embryo trunk (dET) ≈ 35 µm^2; no GBP was reported (Rupprecht et al.; 2017). In the *Drosophila* eye antennal disc no GBP was described (dEA folded; MACAs ≈ 33 µm^2, dEA non-folded; MACAs ≈ 39 µm^2) (Ku and Sun; 2017). It is unknown if GBP takes place in the *Drosophila* pre-pupal WD after puparium formation (dWP 4–7 APF) (Diaz-de-la Loza et al.; 2018); MACAs increase from 8 µm^2 4h APF to 16 µm^2 7h APF. No GBP was reported in mouse outer hair cells (mOHC1–3 P1,3,5,7.5); MACAs decrease from 35 µm^2 (P1) to 16 µm^2 (P7.5). No GBP takes place in the inner hair cells (mIHC1 P1,3,6,7.5); MACAs decrease from 54 µm^2 (P1) to 29 µm^2 (P7.5) (Etournay et al.; 2010). No GBP was reported in the mouse-ear epidermis (mEE), with MACAs of 1044 µm^2 (Yokouchi et al.; 2016).

concentration over larger regions than a single cell area barely reduces the sensed variability (Fig. 2E).

In summary, larger cross-sectional cell diameters increase the variability of the morphogen concentration profiles, while spatial averaging over the cell surface barely reduces the gradient variability. Spatial averaging may, however, counteract detection noise at low morphogen concentrations far away from the source. It is currently unknown over which distance morphogen gradients operate. At distance 12λ from the source, for instance, exponential concentrations will have declined by 160-thousand-fold. At such low levels, detection noise may dominate readout variability unless removed by spatial averaging.

Positional error remains low even at large distance from the source

In our simulations at prescribed mean gradient decay length μ_λ, we observe that the positional error of the gradient, σ_x, increases with the square root of the mean cell diameter, μ_δ:

$$\frac{\sigma_x}{\mu_\lambda} \sim \sqrt{\frac{\mu_\delta}{\mu_\lambda}}, \tag{3}$$

or equivalently,

$$\frac{\sigma_x}{\mu_\delta} \sim \sqrt{\frac{\mu_\lambda}{\mu_\delta}}, \tag{4}$$

with a prefactor that increases with the readout position along the patterning axis (Fig. 2F). The proportionality prefactor in Eqs. 3 and 4 is below 1 even at a readout distance of 12λ from the source, and further reduces towards it. The relationships in Eqs. 3, 4 are in agreement with the previous observation that $\sigma_x/\mu_\lambda \sim (\mu_x/\mu_\lambda)\,\mathrm{CV}_\lambda$ for small CV_0 (Vetter and Iber; 2021, Eq. 9), when we plug in the relationship $\mathrm{CV}_\lambda \sim \sqrt{\mu_\delta/\mu_\lambda}$ found in Eq. 2. Incidentally, the deterministic limit ($\mathrm{CV}_C \to 0$, $\sigma_x \to 0$) is recovered in the continuum limit $\mu_\delta \to 0$.

The lowest relative cell diameter μ_δ/μ_λ that we are aware of is 1/9 for the FGF8 gradient in zebrafish (Yu et al.; 2009).

The results in Fig. 2F then suggest that the positional error is lower than a third of the decay length, $\sigma_x/\mu_\lambda < 1/3$, or smaller than three cell diameters, $\sigma_x/\mu_\delta < 3$, over a spatial extent of 12λ. Closer to the source, and in systems with larger μ_δ/μ_λ ratio, the relative positional error will be lower and can fall well below one cell diameter. For the SHH gradient in the mouse NT, $\mu_\delta/\mu_\lambda = 1/4$ (Cohen et al.; 2015; Kicheva et al.; 2014), and thus $\sigma_x/\mu_\delta < 2$ over 12λ.

We conclude that the positional error is less than one cell diameter in case of wide cells, and somewhat above one cell diameter for narrower cells over the entire range of reasonable readout positions. The highest *absolute* patterning precision (σ_x) is nonetheless achieved for narrow cells as the patterning resolution is low with wide cells.

Tissues that use gradient-based patterning have small apical cell areas

We wondered whether cell diameters would be small in tissues that rely on gradient-based patterning (GBP), so we collected mean apical cell areas for a wide range of tissues from the literature (Fig. 2G). The data confirms that apical cell areas are small in tissues that employ GBP. Our theory makes no prediction about the apical areas in tissues that do *not* employ GBP, but in all cases that we have checked, apical areas are larger and appear to further increase in later developmental stages and in adult animals.

3 Discussion

Using simulations, we have shown that gradient precision decreases with increasing cross-sectional area of the patterned cells. Consistent with our prediction, apical surface areas are small in epithelia that employ gradient-based patterning. Interestingly, signalling by Dpp, the fly homolog of mammalian BMP2/4, results in taller cells with smaller cross-sectional area in its patterning domain compared to other parts of the *Drosophila* wing disc (Widmann and Dahmann; 2009; Legoff et al.; 2013; Bai et al.; 2013). The apical areas are almost twofold smaller close to the source, and increase roughly linearly with distance from it to the Dpp signalling range limit (Legoff et al.; 2013). Similarly, the morphogens SHH and WNT have been observed to increase cell height and reduce the cell cross-sectional area via their impact on actin polymerisation, myosin localisation and activity in the embryonic mouse NT and lung (Kadzik et al.; 2014; Widmann and Dahmann; 2009; Gritli-Linde et al.; 2002; Kondo and Hayashi; 2015; Chiang et al.; 1996). In light of our study, it is possible that the morphogen-dependent reduction in the cross-sectional cell area via positive modulation of cell height serves to enhance patterning precision. Moreover, in curved domains, precision will be higher on the inside, where the average cell diameter is smaller. In the mouse NT, the SHH-sensing cilium is indeed located on the inner, apical surface (Saade et al.; 2013).

We have revealed square-root scaling relationships between the positional error, cell diameter and gradient decay length in Eqs. 3 and 4. These relationships predict that exponential morphogen gradients remain highly accurate over very long distances, providing highly accurate positional information even far away from the morphogen source. Our results are system-agnostic, and could apply widely in development.

Methods

Numerical simulation of noisy gradients

Noisy gradients were obtained by solving a one-dimensional steady-state reaction-diffusion system, as developed by Vetter and Iber (2021), given by the boundary value problem

$$pH(-x) - dC(x) = -D\frac{\partial^2 C(x)}{\partial x^2} \tag{5}$$

with zero-flux boundary conditions

$$\frac{\partial C(-L_\mathrm{s})}{\partial x} = 0 = \frac{\partial C(L_\mathrm{p})}{\partial x}.$$

Eq. 5 contains a source term with production rate p, a linear sink term with degradation rate d, and a Fickian diffusion term with diffusion coefficient D. It was numerically solved on a discrete domain consisting of two subdomains, a source domain on the interval $-L_\mathrm{s} \leq x \leq 0$ and a patterning domain on the interval $0 \leq x \leq L_\mathrm{p}$, (Fig. 1B). A mean cell diameter of $\mu_\delta = 5$ µm was chosen as in Cohen et al. (2015). We used $L_\mathrm{s} = 5\mu_\delta$ and $L_\mathrm{p} = 50\mu_\delta$, with exception of Fig. 2E and Fig. 2F where $L_\mathrm{p} = 65\mu_\delta$ to allow for readout positions far away from the source. The Heaviside step function $H(-x)$ ensures that production only occurs in the source, whereas degradation is assumed to take place over the whole domain. The kinetic parameters $k = p, d, D$ were drawn for each cell independently from log-normal distributions with prescribed mean values μ_k and respective coefficients of variation CV_k (see Vetter and Iber (2021) for details). We fixed molecular variability at the physiological value $\mathrm{CV}_k = 0.3$ (Vetter and Iber; 2021) here. As a new source of noise, cell size variability was introduced. Since the cell area distributions in the *Drosophila* larval & prepupal wing discs and in the mouse NT resemble log-normal distributions (Sánchez-Gutiérrez et al.; 2016; Guerrero et al.; 2019), we drew individual cell areas A independently from a log-normal distribution with prescribed mean μ_A and coefficient of variation CV_A. They were then converted to diameters δ according to $\delta = 2\sqrt{A/\pi}$. To control the mean cell diameter μ_δ as used in the figures and equations, the mean cell area was calculated as $\mu_A = \pi(\mu_\delta/2)^2\sqrt[4]{1+\mathrm{CV}_A^2}$ for given μ_δ and CV_A, as follows from the transformation properties of log-normal random variables.

Each data point in the figures corresponds to the mean ± SEM of 1000 independent simulations with random parameters. For each generated morphogen gradient, the two coefficients λ and C_0 were extracted by fitting hyperbolic cosines to the logarithmised numerical solution as detailed in Vetter and Iber (2021).

Code Availability

The source code is publicly released under the 3-clause BSD license as a git repository at `https://git.bsse.ethz.ch/iber/Publications/2022_adelmann_vetter_cell_size`.

Acknowledgements

We thank Marco Meer for providing cell area data, Fernando Casares and Nikolaos Doumpas for discussions. This work was funded by SNF Sinergia grant CRSII5_170930.

Competing Interests

The authors declare no competing interests.

Author Contributions

RV & DI conceived the study, JA and RV developed the numerical framework and produced the figures, JA carried out the simulations and analysis, RV developed the theory, DI contributed the supporting data. All authors wrote the manuscript.

References

Akieda, Y., Ogamino, S., Furuie, H., Ishitani, S., Akiyoshi, R., Nogami, J., Masuda, T., Shimizu, N., Ohkawa, Y. and Ishitani, T. (2019). Cell competition corrects noisy Wnt morphogen gradients to achieve robust patterning in the zebrafish embryo, *Nat. Commun.* p. 4710.

Bai, L., Widmann, T., Jülicher, F., Dahmann, C. and Breen, D. (2013). 3D surface reconstruction and visualization of the *Drosophila* wing imaginal disc at cellular resolution, *Proc. SPIE* 8654: 86540D.

Berg, H. C. and Purcell, E. M. (1977). Physics of chemoreception, *Biophys. J.* 20: 193–219.

Bialek, W. and Setayeshgar, S. (2005). Physical limits to biochemical signaling, *Proceedings of the National Academy of Sciences* 102(29): 10040–10045.

Bocanegra-Moreno, L., Singh, A., Hannezo, E., Zagorski, M. and Kicheva, A. (2022). Cell cycle dynamics controls fluidity of the developing mouse neuroepithelium, *bioRxiv* .

Briscoe, J. and Small, S. (2015). Morphogen rules: design principles of gradient-mediated embryo patterning, *Development* 142: 3996–4009.

Cavodeassi, F., Rodrígguez, I. and Modolell, J. (2002). Dpp signalling is a key effector of the wing-body wall subdivision of the *Drosophila* mesothorax, *Development* 129: 3815–3823.

Chiang, C., Litingtung, Y., Lee, E., Young, K. E., Corden, J. L., Westphal, H. and Beachy, P. A. (1996). Cyclopia and defective axial patterning in mice lacking *Sonic hedgehog* gene function, *Nature* 383: 407–413.

Cohen, M., Kicheva, A., Ribeiro, A., Blassberg, R., Page, K. M., Barnes, C. P. and Briscoe, J. (2015). Ptch1 and Gli regulate Shh signalling dynamics via multiple mechanisms, *Nat. Commun.* 6: 6709.

Diaz-de-la Loza, M.-d.-C., Ray, R. P., Ganguly, P. S., Alt, S., Davis, J. R., Hoppe, A., Tapon, N., Salbreux, G. and Thompson, B. J. (2018). Apical and Basal Matrix Remodeling Control Epithelial Morphogenesis, *Dev. Cell* 46: 23–39.e5.

Escudero, L. M., Costa Lda, F., Kicheva, A., Briscoe, J., Freeman, M. and Babu, M. M. (2011). Epithelial organisation revealed by a network of cellular contacts, *Nat. Commun.* 2: 526.

Etournay, R., Lepelletier, L., Boutet de Monvel, J., Michel, V., Cayet, N., Leibovici, M., Weil, D., Foucher, I., Hardelin, J. P. and Petit, C. (2010). Cochlear outer hair cells undergo an apical circumference remodeling constrained by the hair bundle shape, *Development* 137: 1373–1383.

Finegan, T. M., Na, D., Cammarota, C., Skeeters, A. V., Nadasi, T. J., Dawney, N. S., Fletcher, A. G., Oakes, P. W. and Bergstralh, D. T. (2019). Tissue tension and not interphase cell shape determines cell division orientation in the *Drosophila* follicular epithelium, *EMBO J.* 38.

Gómez, H. F., Dumond, M. S., Hodel, L., Vetter, R. and Iber, D. (2021). 3D cell neighbour dynamics in growing pseudostratified epithelia, *eLife* 10: e68135.

Gregor, T., McGregor, A. P. and Wieschaus, E. F. (2008). Shape and function of the Bicoid morphogen gradient in dipteran species with different sized embryos, *Dev. Biol.* 316: 350–358.

Gregor, T., Tank, D. W., Wieschaus, E. F. and Bialek, W. (2007). Probing the Limits to Positional Information, *Cell* 130: 153–164.

Gritli-Linde, A., Bei, M., Maas, R., Zhang, X. M., Linde, A. and McMahon, A. P. (2002). Shh signaling within the dental epithelium is necessary for cell proliferation, growth and polarization, *Development* 129: 5323–5337.

Guerrero, P., Perez-Carrasco, R., Zagorski, M., Page, D., Kicheva, A., Briscoe, J. and Page, K. M. (2019). Neuronal differentiation influences progenitor arrangement in the vertebrate neuroepithelium, *Development* 146: dev176297.

Houchmandzadeh, B., Wieschaus, E. and Leibler, S. (2002). Establishment of developmental precision and proportions in the early *Drosophila* embryo, *Nature* 415: 798–802.

Iber, D. (2021). The Control of Lung Branching Morphogenesis, *Cellular Networks in Development*, Vol. 143 of *Current Topics in Developmental Biology*, Elsevier, chapter 6, pp. 205–237.

Kadzik, R. S., Cohen, E. D., Morley, M. P., Stewart, K. M., Lu, M. M. and Morrisey, E. E. (2014). Wnt ligand/Frizzled 2 receptor signaling regulates tube shape and branch-point formation in the lung through control of epithelial cell shape, *Proceedings of the National Academy of Sciences of the United States of America* 111: 12444–12449.

Kicheva, A., Bollenbach, T., Ribeiro, A., Valle, H. P., Lovell-Badge, R., Episkopou, V. and Briscoe, J. (2014). Coordination of progenitor specification and growth in mouse and chick spinal cord, *Science* 345.

Kicheva, A., Pantazis, P., Bollenbach, T., Kalaidzidis, Y., Bittig, T., Jülicher, F. and González-Gaitán, M. (2007). Kinetics of Morphogen Gradient Formation, *Science* 315: 521–525.

Kim, Y. K., Yu, H., Summers, V. R., Donaldson, K. J., Ferdous, S., Shelton, D., Zhang, N., Chrenek, M. A., Jiang, Y., Grossniklaus, H. E., Boatright, J. H., Kong, J. and Nickerson, J. M. (2021). Morphometric Analysis of Retinal Pigment Epithelial Cells From C57BL/6J Mice During Aging, *Invest. Ophth. Vis. Sci.* 62: 32.

Kokic, M., Iannini, A., Villa-Fombuena, G., Casares, F. and Iber, D. (2019). Minimisation of surface energy drives apical epithelial organisation and gives rise to Lewis' law, *bioRxiv* .

Kondo, T. and Hayashi, S. (2015). Mechanisms of cell height changes that mediate epithelial invagination, *Dev. Growth Differ.* 57: 313–323.

Ku, H.-Y. and Sun, Y. H. (2017). Notch-dependent epithelial fold determines boundary formation between developmental fields in the *Drosophila* antenna, *PLOS Genet.* 13: 1–30.

Lander, A. D., Lo, W.-C., Nie, Q. and Wan, F. Y. M. (2009). The Measure of Success: Constraints, Objectives, and Tradeoffs in Morphogen-mediated Patterning, *CSH Perspect. Biol.* 1.

Legoff, L., Rouault, H. and Lecuit, T. (2013). A global pattern of mechanical stress polarizes cell divisions and cell shape in the growing *Drosophila* wing disc, *Development* 140: 4051–4059.

Mateus, R., Holtzer, L., Seum, C., Hadjivasiliou, Z., Dubois, M., Jülicher, F. and Gonzalez-Gaitan, M. (2020). BMP Signaling Gradient Scaling in the Zebrafish Pectoral Fin, *Cell. Rep.* 30: 4292–4302 e7.

Morishita, Y. and Iwasa, Y. (2009). Accuracy of positional information provided by multiple morphogen gradients with correlated noise, *Phys. Rev. E* 79: 061905.

Morishita, Y. and Iwasa, Y. (2011). Coding Design of Positional Information for Robust Morphogenesis, *Biophys. J.* 101: 2324–2335.

Osterfield, M., Berg, C. A. and Shvartsman, S. Y. (2017). Epithelial Patterning, Morphogenesis, and Evolution: *Drosophila* Eggshell as a Model, *Dev. Cell* 41: 337–348.

Pera, E., Stein, S. and Kessel, M. (1999). Ectodermal patterning in the avian embryo: epidermis versus neural plate, *Development* 126: 63–73.

Rupprecht, J. F., Ong, K. H., Yin, J., Huang, A., Dinh, H. H., Singh, A. P., Zhang, S., Yu, W. and Saunders, T. E. (2017).

Geometric constraints alter cell arrangements within curved epithelial tissues, *Mol. Biol. Cell* 28: 3582–3594.

Saade, M., Gutierrez-Vallejo, I., Le Dreau, G., Rabadan, M. A., Miguez, D. G., Buceta, J. and Marti, E. (2013). Sonic Hedgehog Signaling Switches the Mode of Division in the Developing Nervous System, *Cell Rep.* 4: 492–503.

Saitoh, M., Shirakihara, T., Fukasawa, A., Horiguchi, K., Sakamoto, K., Sugiya, H., Beppu, H., Fujita, Y., Morita, I., Miyazono, K. and Miyazawa, K. (2013). Basolateral BMP Signaling in Polarized Epithelial Cells, *PLoS One* 8: e62659.

Sánchez-Gutiérrez, D., Tozluoglu, M., Barry, J. D., Pascual, A., Mao, Y. and Escudero, L. M. (2016). Fundamental physical cellular constraints drive self-organization of tissues, *EMBO J.* 35: 77–88.

Skouloudaki, K., Papadopoulos, D. K., Tomancak, P. and Knust, E. (2019). The apical protein Apnoia interacts with Crumbs to regulate tracheal growth and inflation, *PLoS Genet.* 15: e1007852.

Tkačik, G., Dubuis, J. O., Petkova, M. D. and Gregor, T. (2015). Positional Information, Positional Error, and Readout Precision in Morphogenesis: A Mathematical Framework, *Genetics* 199: 39–59.

Tomoyasu, Y., Ueno, N. and Nakamura, M. (2000). The Decapentaplegic morphogen gradient regulates the notal *wingless* expression through induction of *pannier* and *u-shaped* in *Drosophila*, *Mechanisms of Development* 96: 37–49.

Tsai, T. Y.-C., Sikora, M., Xia, P., Colak-Champollion, T., Knaut, H., Heisenberg, C.-P. and Megason, S. G. (2020). An adhesion code ensures robust pattern formation during tissue morphogenesis, *Science* 370: 113–116.

Vetter, R. and Iber, D. (2021). Inference of Morphogen Gradient Precision from Molecular Noise Data, *bioRxiv* .

Wartlick, O., Jülicher, F. and Gonzalez-Gaitan, M. (2014). Growth control by a moving morphogen gradient during *Drosophila* eye development, *Development* 141: 1884–1893.

Wartlick, O., Mumcu, P., Kicheva, A., Bittig, T., Seum, C., Jülicher, F. and González-Gaitán, M. (2011). Dynamics of Dpp Signaling and Proliferation Control, *Science* 331: 1154–1159.

Widmann, T. J. and Dahmann, C. (2009). Dpp signaling promotes the cuboidal-to-columnar shape transition of *Drosophila* wing disc epithelia by regulating Rho1, *J. Cell Sci.* 122: 1362–1373.

Wolpert, L. (1969). Positional information and the spatial pattern of cellular differentiation, *J. Theor. Biol.* 25: 1–47.

Xiong, F., Tentner, A. R., Huang, P., Gelas, A., Mosaliganti, K. R., Souhait, L., Rannou, N., Swinburne, I. A., Obholzer, N. D., Cowgill, P. D., Schier, A. F. and Megason, S. G. (2013). Specified Neural Progenitors Sort to form Sharp Domains after Noisy Shh Signaling, *Cell* 153: 550–561.

Yokouchi, M., Atsugi, T., Logtestijn, M. v., Tanaka, R. J., Kajimura, M., Suematsu, M., Furuse, M., Amagai, M. and Kubo, A. (2016). Epidermal cell turnover across tight junctions based on kelvin's tetrakaidecahedron cell shape, *eLife* 5: e19593.

Yu, S. R., Burkhardt, M., Nowak, M., Ries, J., Petrasek, Z., Scholpp, S., Schwille, P. and Brand, M. (2009). Fgf8 morphogen gradient forms by a source-sink mechanism with freely diffusing molecules, *Nature* 461: 533–536.

Zagorski, M., Tabata, Y., Brandenberg, N., Lutolf, M. P., Tkačik, G., Bollenbach, T., Briscoe, J. and Kicheva, A. (2017). Decoding of position in the developing neural tube from antiparallel morphogen gradients, *Science* 356: 1379–1383.

Zhang, Z., Zwick, S., Loew, E., Grimley, J. S. and Ramanathan, S. (2019). Mouse embryo geometry drives formation of robust signaling gradients through receptor localization, *Nat. Commun.* 10: 4516.